JPE 17-5-15

https://doi.org/10.6113/JPE.2017.17.5.1278
ISSN(Print): 1598-2092 / ISSN(Online): 2093-4718

Grid-friendly Characteristics Analysis and Implementation of a Single-phase Voltage-controlled Inverter

Shuaitao Zhang*, Jinbin Zhao†, Yang Chen*, and Chaojie He*

*, †College of Electrical Engineering, Shanghai University of Electric Power, Shanghai, China

Abstract

Inverters are widely used in distributed power generation and other applications. However, their lack of inertia and variable impedance may cause system instability and power transfer inaccuracy. This paper proposes a control scheme for a single phase voltage-controlled inverter with some grid-friendly characteristics. The proposed control algorithm enables the inverter to function as a voltage source with an inner output impedance in both the islanded and grid-connected modes. Virtual inertia and rotor equations are embedded in the PLL part. Thus, the frequency stability can remain. The inner output impedance can be adjusted freely, which helps to accurately decouple and transmit the output active and reactive power. The proposed inverter operates like a traditional synchronous generator. Simulations and experiments are designed and carried out to verify the proposed control strategy.

Key words: Microgrid, Output impedance, Virtual inertia, Voltage-controlled inverter

I. INTRODUCTION

Power electronic devices are enjoying increasing popularity due to the development of smartgrids and distributed generations. It is easier to absorb distributed generators such as photovoltaic cells, wind turbines and fuel cells into microgrids with power converters (also called inverters) [1]-[3].

Inverters are usually the key device in microgrid applications. According to the authors of [4], inverters can be classified into three categories: grid-feeding, grid-supporting, and grid-forming. Both voltage-controlled inverters (VCIs) and current-controlled inverters (CCIs) can be used for grid-feeding in the grid-connected mode [5]-[9]. VCIs are inverters that can adjust the output voltage amplitude, frequency and phase to desired values, while CCIs inject current into a grid, so that the amplitude, frequency and phase are regulated to desired values. CCIs cannot supply loads independently as VCIs do. Thus, they cannot work for grid-forming. On the other hand, microgrids do not have many traditional synchronous generators for grid supporting or grid forming. When grid faults occur, microgrids work in the islanded mode and become easy to collapse [10]. Commonly used CCIs are grid-feeding inverters. They perform like current sources and cannot transfer power to the load without the support of grid. While VCIs are grid-supporting inverters and they can be treated as voltage sources which can provide voltage support in urgent circumstances.

Microgrid inverters often operate in parallel without interconnection. Therefore, the P-f droop control which mimics the output characteristics of a traditional synchronous generator is widely adopted. However, the droop control method usually does not consider the effects of the high penetration of distributed generation. Specifically, the conditions of the whole grid may deteriorate or even crash because of the high penetration of distributed renewable energy and the lack of inertia in microgrid systems [11]. In this case, methods to improve grid-connected inverter control strategies to achieve friendly access of distributed generation in large-scale applications have become key issues to be solved. Control strategies referred to as Virtual Synchronous Generators (VSG) have been developed [12]-[15] to solve these problems. The model of a traditional synchronous

Manuscript received Aug. 8, 2016; accepted Jun. 15, 2017
Recommended for publication by Associate Editor Sung-Jin Choi.
†Corresponding Author: zhaojinbin@shiep.edu.cn
Tel: +86-189-6485-8856, Shanghai University of Electric Power
*College of Electrical Eng., Shanghai University of Electric Power, China

generator is simulated by VSG technology, which increases the inertia of a microgrid and improves its stability. The authors of [14] introduced the idea of a VSG based on a rotor equation. The concept of 'synchronverter' is well known nowadays. It is a converter that mimics both the inertial equation and electromagnetic transient process of synchronous generators. However, the output impedance of the inverter is a real filter inductor and is not controllable. In addition, there is no detailed discussion of the inertial equation. Many VSG strategies mixed p and f controllers together. Thus, the analysis of the traditional phase locked loop is more complex. Line impedance and grid equivalent impedance are variables in microgrids, which makes power control difficult to realize. Nowadays, inverters often adopt a virtual impedance to realize power control [15]-[18]. The authors of [15] introduced an adaptive impedance control strategy based on active and reactive power change. This control strategy has an excellent dynamic response. However, it is quite complex and hard to realize in practice. The authors of [19] proposed a novel control strategy for inverters in microgrids. The inverter has some grid friendly characteristics. However, the analysis is simple and requires further development.

This paper proposes a control strategy of a flexible voltage controlled inverter (FVCI) which provides both inner output impedance and flexible voltage. In addition, it has some similar characteristics of VSG. Precisely, the inverter has two axial voltage regulators. The first regulator controls the output voltage amplitude and the second controls the output frequency. The output impedance can be regulated freely by setting certain control parameters. The output impedance helps to manage the active and reactive power flow. If the chosen output impedance inductive is big enough, the active and reactive power can be decoupled well as traditional synchronous generators do.

The following parts are arranged as follows. Part II talks about the whole system and the control method of the proposed voltage control algorithm with an inner output impedance. A detailed discussion of the frequency regulation, which possesses virtual inertia, is presented in Part III. Part IV presents results of simulations and experiments to verify the strategy. Finally, some conclusions are given in Part V.

II. System Description and Control Scheme

The main circuit of the FVCI is shown in Fig. 1. V_{DC} is the power supply from renewable energy sources. Since this is not the focus of this paper, the DC source is treated as a constant value. A single-phase full bridge converter is applied. An LCL filter is used and a small resistor is cascaded with the capacitor to decrease possible oscillations.

The role of the control circuit is to produce appropriate gate signals for the four main switches. Fig. 2 indicates the cascaded structure of the control system. The top block consists 2 parts: the 1st and 2nd axial voltage regulators. These two reference

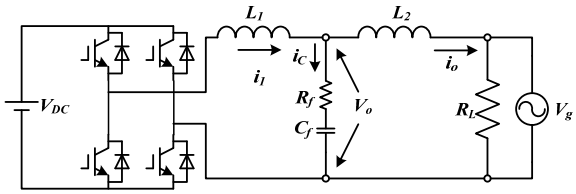

Fig. 1. Main circuit of the FVCI.

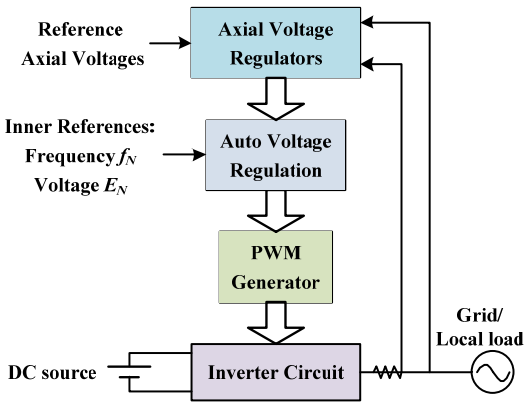

Fig. 2. General control scheme.

values adjust the inverter output voltage in islanded and grid-connected modes. v_{m1}, the output of the 1st axial voltage regulator, controls the voltage amplitude. v_{m2}, the output of the 2nd regulator, controls the output frequency. When the inverter works in the PQ control mode, the two regulators can independently control the output active and reactive power with proper parameters design [20]. The auto voltage regulation block consists of two main parts: the frequency regulation as well as the voltage and impedance regulation. This gives the PWM generator reference current so that the whole system works as a desired AC voltage source with a proper inner output impedance. Two basic parameters are set in this block: the basic frequency ω_N and the basic output voltage E_N. When the inverter is working under the islanded mode, its output voltage amplitude and frequency are kept at basic values. The main circuit at the bottom has already been shown in Fig. 1. The inner current loop with the SPWM is used as a PWM generator. Because of the oscillation resistor R_f, control stability is easy to achieve.

The detailed control scheme is shown in Fig. 3. In the main circuit, an LCL filter is adopted and L_2 is small. As a result, the capacitor voltage v_o is almost the same as the grid voltage v_g. V_1^* and V_2^* are reference values for the axial voltage regulators. When working in the islanded mode, the former regulator controls the output voltage amplitude, while the latter controls the frequency. The quadrature voltage v_q can be obtained with an orthogonal transformation. After adding v_{m2} from the 2nd axial voltage regulator, v_{qq} is sent to a 1-order inertial unit. Details of the PLL part are presented in the following part.

i_o and v_o are measured for auto voltage regulation. The regulation block contains three parts: the voltage feedback loop, the capacitor current loop, and the output current feedforward

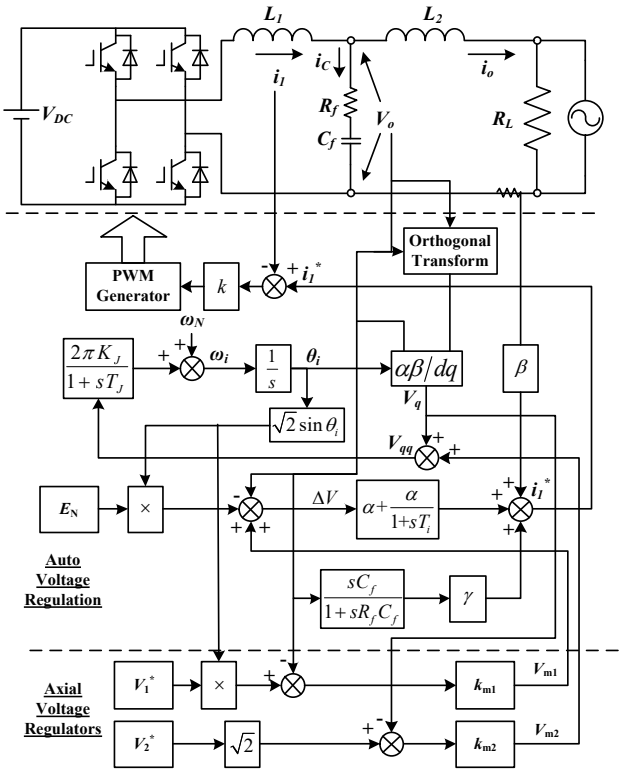

Fig. 3. Detailed control scheme of the FVCI.

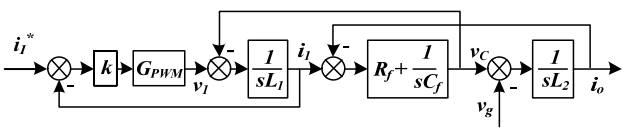

Fig. 4. Inner PWM generation.

loop. The voltage feedback loop contains a proportional and integral circuit, where α is the feedback gain and T_i is the integral time constant. The capacitor current is compensated by adding the fundamental component, which is calculated by its voltage, to the PWM reference. The output current i_o is added to the PWM reference as a feedforward value. The feedforward gain is β. The current running through the inverter side inductor is adopted for the PWM generation part.

The PWM generator reference i_1^* is generated as bellow. Eqn. 1 can be derived from Fig. 3.

$$I_1(s) = I_o(s) + V_o(s)\frac{sC_f}{1+sR_fC_f} \tag{1}$$

The voltage and impendence regulation part generates the PWM reference i_1^* as bellow.

$$\begin{aligned} I_1^*(s) &= \alpha\left(1+\frac{1}{sT_i}\right)\left(V_E(s)-(1+k_{m1})V_o(s)\right) \\ &+ \beta I_o(s) + \gamma V_o(s)\frac{sC_f}{1+sR_fC_f} \end{aligned} \tag{2}$$

Where $v_E(t) = \sqrt{2}\left(E + k_{m1}V_1^*\right)\sin\theta_i$

Fig. 4 is a control block of the inner PWM generation.

In the control block, the inner PWM generation loop satisfies Eqn. 3. After rewriting Eqn. 3, Eqn. 4 can be obtained. From Eqn. 4, G_{PWM} is chosen large enough so that the PWM generator works as a current follower and Eqn. 5 is satisfied. This greatly simplifies the following theoretical analysis.

$$\left(\left(I_1^* - I_1\right)G_{PWM} - V_C\right)\frac{1}{sL_1} = I_1 \tag{3}$$

$$I_1 = \frac{G_{PWM}}{G_{PWM}+sL_1}I_1^* - \frac{V_C}{G_{PWM}+sL_1} \tag{4}$$

$$I_1(s) = I_1^*(s) \tag{5}$$

Solving Eqns. 1, 2 and 5 simultaneously, V_o(s) is obtained as follows.

$$\begin{aligned} V_o(s) = &\frac{\alpha\left(1+\frac{1}{sT_i}\right)}{\alpha(1+k_{m1})\left(1+\frac{1}{sT_i}\right)+(1-\gamma)\frac{sC_f}{1+sR_fC_f}}V_E(s) \\ &- \frac{1-\beta}{\alpha(1+k_{m1})\left(1+\frac{1}{sT_i}\right)+(1-\gamma)\frac{sC_f}{1+sR_fC_f}}I_o(s) \end{aligned} \tag{6}$$

Eqn. 6 indicates that the output capacitor voltage depends on both V_E and the output current I_o. V_E determines the first item while I_o determines the latter. When the output current I_o is 0, the output voltage is equivalent to the first item. That is the equivalent electromotive force of the inverter. The second term suggests that the output voltage decreases proportionally to the output current. This means that the coefficient of the second term is the inner output impedance of the designed inverter.

If γ is chosen as 1, Eqn. 6 is greatly simplified to Eqn. 7 as follows.

$$V_o(s) = \frac{V_E(s)}{1+k_{m1}} - \frac{1-\beta}{\alpha(1+k_{m1})\left(1+\frac{1}{sT_i}\right)}I_o(s) \tag{7}$$

From Eqn. 7, the expressions of the electromotive force V_i and the inner output conductance Y_i are obtained as follows.

$$V_i(t) = \frac{V_E(t)}{1+k_{m1}} = \sqrt{2}\frac{E+k_{m1}V_1^*}{1+k_{m1}}\sin\theta_i \tag{8}$$

$$Y_i(s) = \frac{\alpha(1+k_{m1})}{1-\beta}\left(1+\frac{1}{sT_i}\right) \tag{9}$$

Eqns. 8 and 9 mean that the inverter has the equivalent circuit indicated in Fig. 5, where:

$$R_i = \frac{1-\beta}{\alpha(1+k_{m1})} \tag{10}$$

$$L_i = R_iT_i \tag{11}$$

The circuit in Fig. 5 is valid for both small signal operation and large signal operation. The output voltage and impedance are nearly determined by the control parameters. The output impedance consists of a resistor and a paralleled inductor. If T_i is chosen to be not zero but small enough, the output impedance is mainly inductive.

β is another parameter that controls the output impedance.

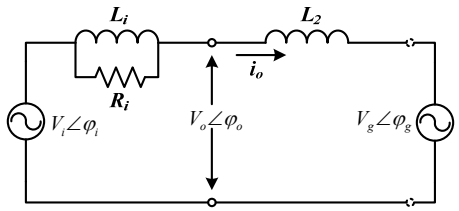

Fig. 5. Equivalent circuit of the system.

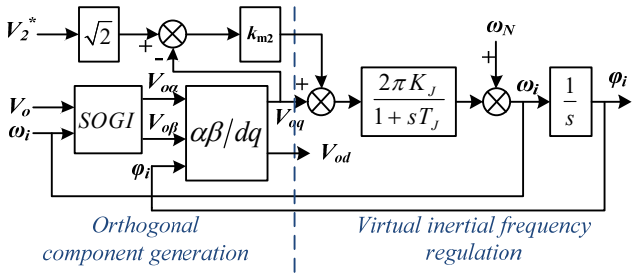

Fig. 6. Control block of the frequency regulation.

It can be positive or negative as well. If β is chosen to be equal to 1, the output impedance is zero. This is a good characteristic for UPS applications.

III. Frequency Regulation

The traditional synchronous generator itself has a large inertia. Therefore, the voltage frequency does not have a considerable drop or increase when the load greatly changes. Droop control is widely used in microgrids. However, the frequency may have sharp fluctuations when the load greatly changes. This harms the frequency stability of a microgrid. With the inertia embedded in the PLL part, the frequency stability of the FVCI remains good. The PLL part consists of two parts: the orthogonal component generation part and the virtual inertial frequency regulation part. First, the capacitor voltage is measured. Then the orthogonal component of the voltage is generated and sent to the transform block with the original voltage. Another key component of the PLL is the inertial element. It produces a virtual inertia for the inverter. The detailed mathematical analysis is shown below.

Choose a value of L_2 which is small enough so that $v_o \approx v_g$ can be satisfied. Thus, $v_o(=\sqrt{2}V_o\sin\varphi_o)$ can be replaced by $v_g(=V_g\sin\varphi_g)$ from here. In Fig. 5, assuming that $\delta=\varphi_i-\varphi_o$, then the output power can be written as:

$$\begin{cases} P_e = \dfrac{E_i V_o}{X}\sin\delta \\ Q_e = \dfrac{E_i V_o\cos\delta - V_o^2}{X} \end{cases} \tag{12}$$

E_i, V_o and X can be regarded as constant values. Hence, $V_o\sin\delta$ contains the output active power information. It represents the value of P_e. $V_o\sin\delta$ can be obtained from a $\alpha\beta/dq$ transformation. The frequency control strategy is shown in Fig. 6. It has some great characteristics which are analyzed below.

A. Self-Synchronization Ability Analysis

The output voltage $V_o\sin\varphi_o$ has been measured to get the phase information. Here the secondary order generalized integrator (SOGI) algorithm is used to generate the orthogonal components of v_o. Analyze this control block and some formulas can be deduced as follows.

$$V_{o\alpha} = \sqrt{2}V_o\sin\varphi_o \tag{13}$$

$$V_{o\beta} = \sqrt{2}V_o\sin\left(\varphi_o - \frac{\pi}{2}\right) = -\sqrt{2}V_o\cos\varphi_o \tag{14}$$

Given $\delta(t)=\varphi_i-\varphi_g\approx 0$,

$$\begin{aligned} V_{oq} &= V_{o\alpha}\cos\varphi_i + V_{o\beta}\sin\varphi_i \\ &= -\sqrt{2}V_o\sin(\varphi_o-\varphi_i) \approx \sqrt{2}V_o(\varphi_o-\varphi_i) \end{aligned} \tag{15}$$

According to Fig 6, the following equation is satisfied.

$$V_{oq}(s) = \sqrt{2}V_o(\varphi_o(s)-\varphi_i(s)) = \sqrt{2}V_o\left(\frac{\omega_o}{s^2} - \frac{\omega_i(s)}{s} - \frac{\delta(0)}{s}\right) \tag{16}$$

$$\omega_i(s) = \left(\frac{\sqrt{2}k_{m2}V_2^*}{s} + (1-k_{m2})V_{oq}(s)\right)\frac{2\pi K_J}{1+sT_J} + \frac{\omega_N}{s} \tag{17}$$

ω_i can be calculated by solving Eqn. 16 and 17. ω_g is the grid angular frequency.

$$\omega_i(s) = \frac{\dfrac{\sqrt{2}k_{m2}V_2^*}{s} + \dfrac{\sqrt{2}(1-k_{m2})V_o}{s^2}\omega_g}{\dfrac{1+sT_J}{2\pi K_J} + \dfrac{\sqrt{2}(1-k_{m2})V_o}{s}} + \frac{\dfrac{1+sT_J}{s2\pi K_J}\omega_N - \dfrac{\sqrt{2}(1-k_{m2})V_o}{s}\delta(0)}{\dfrac{1+sT_J}{2\pi K_J} + \dfrac{\sqrt{2}(1-k_{m2})V_o}{s}} \tag{18}$$

The steady state value is calculated as Eqn. 19.

$$\lim_{t\to\infty}\omega_i(t) = \lim_{s\to 0}s\omega_i(s) = \omega_g \tag{19}$$

The steady state value of the output frequency is not related to the reference value ω_N. It is eventually equal to the frequency of the PCC.

Usually, the power angle δ determines the output power. The steady state value of δ is calculated as follows.

$$\delta(s) = \varphi_i(s) - \varphi_g(s) = \frac{\omega_i(s)}{s} - \frac{\omega_g}{s^2} + \frac{\delta(0)}{s} \tag{20}$$

$$\lim_{t\to\infty}\delta(t) = \lim_{s\to 0}s\delta(s) = \frac{k_{m2}V_2^*}{(1-k_{m2})V_o} + \frac{\omega_N-\omega_g}{2\sqrt{2}\pi K_J(1-k_{m2})V_o} \tag{21}$$

Given a certain V_2^* and without a closed loop control, some conclusions can be made from Eqn. 21.

1) In the Grid-Connected Mode: The system frequency ω_g is determined by the grid and the two conclusions below can be made.

1) If $\omega_N>\omega_g$, then δ has an escalating trend, and active power tends to flow from the inverter to the grid. If

$\omega_N<\omega_g$, the power trend is opposite.

2) If $V_2^*>0$, then δ has a rising trend, and active power tends to flow from the inverter to the grid. If $V_2^*<0$, the direction is opposite.

2) In the Islanded Mode or *Microgrid Mode*: Eqn. 12 can often be simplified as follows.

$$P_e = \frac{E_i V_o}{X}\delta \tag{22}$$

By simultaneously solving Eqns. 21 and 22, Eqn. 23 can be obtained.

$$P_e = \frac{E_i}{X}\left(\frac{k_{m2}V_2^*}{(1-k_{m2})} + \frac{\omega_N-\omega_g}{2\sqrt{2}\pi K_J(1-k_{m2})}\right) \tag{23}$$

This adjusting process is discussed in Part B.

The system frequency may drop without a compensation of V_2^* or ω_N when working under the islanded mode. There are two ways to compensate for the frequency drop. For synchronous generators in a big grid, one is called primary regulation and the other is secondary regulation.

B. Rotating Equation and Virtual Inertia Analysis in Microgrids

The inverter has some characteristics of synchronous machines. The PLL part has an embedded synchronous machine rotating equation. The virtual inertia is realized in the structure. The following part analyses this characteristic.

Eqn. 24 is satisfied from Fig. 6.

$$\left(\sqrt{2}V_2^* + (1-k_{m2})V_{oq}(s)\right)\frac{2\pi K_J}{1+sT_J} + \omega_N = \omega_i \tag{24}$$

After rewriting Eqn. 24 in time domain, and marking $\frac{E_i}{2\sqrt{2}\pi K_J(1-k_{m2})X} = D_p$, then Eqn. 25 is satisfied.

$$D_p T_J \frac{d\omega_i}{dt} = P_m - P_e - D_p(\omega_i - \omega_N) \tag{25}$$

In Eqn. 25, $P_m = E_i k_{m2} V_2^* \Big/ \left((1-k_{m2})\sqrt{2}X\right)$, and V_2^* represents the output power command P_m. It can be regarded as AGC (Automatic Generation Control) for synchronous generators. Eqn. 25 has the same format with the rotor equation of the synchronous generator.

Assume that when $t=0^-$, the system is running smoothly with output power P_{e0}. At $t=0^+$, the load changes with a phase step to P_{e1}. Solving Eqn. 19 at $t=0^-\&0^+$, the following equation is satisfied.

$$\Delta\omega_i = \frac{\Delta P_e}{D_p}\left(e^{-\frac{t}{T_J}} - 1\right) \tag{26}$$

There is a built-in *P-f* drop control in the frequency regulation. T_J is the time constant and D_p is the droop coefficient (also called the *difference coefficient* in Power System Analysis). Specifically, T_J reflects the inertia of the system and determines the response time. D_p represents the friction loss to some extent and determines the decrease amplitude. For microgrid applications, T_J should be large enough to restrain the frequency fluctuation. However, T_J cannot be too large. Otherwise it may go beyond the ability of the inverter and cause system instability. If loads with high power quality requirements are connected to the inverter, the coefficient D_P should be smaller for a lower frequency drop.

V_2^* seems like a prime mover. The initial value may come from the MPPT mode or from the upper controller. Just like the adjustment process of large synchronous generators, the proposed inverter has both primary and secondary frequency regulation abilities.

TABLE I
SIMULATION PARAMETERS OF THE MAIN CIRCUIT

V_{DC}/V	320	α	0.2
L_1/mH	5	β	-3
L_2/mH	0.1	γ	1
R_f/Ω	0.5	T_i/ms	0.636
C_f/Ω	22e-6	K_J	0.001
E_N/V	200	T_J/ms	0.2
ω_N/Rad	100π	k_{m1}	1
k	5	k_{m2}	0.5
V_1^*	200	V_2^*	0

IV. SIMULATION AND EXPERIMENTS

A simulation model of the control strategy is built in Matlab/Simulink. The simulation step size is 0.001ms. Fixed step solver ODE 4 Runge-Kutta is adopted. The step size is 0.001ms. The main simulation parameters under the islanded mode and the grid-connected mode are listed in Table I [19]. The rated power of the inverter is 1kVA. Just like the situation of a microgrid, the inverter is directly connected to the main grid with a breaker. No isolation transformer is adopted here. In this paper, two situations have been built to examine the characteristics of the FVCI.

A. In the Islanded Mode or the Microgrid Mode

Fig. 7 shows frequency responses with different T_J and D_p, when t=1.5s and ΔP=0.5kW. In Fig. 7(a), D_p=0.05; and in Fig. 7(b), T_J=0.1s. The larger T_J is, the larger the system inertia is, and the slower the frequency responses. With the same active power change, the frequency drop is proportional to D_p. The T_J and D_P of each inverter may have different stability ranges with different kinds of DC sources.

Fig. 8 shows the difference between the traditional *P-f* droop control [13] and the proposed control strategy under the islanded mode. It is the load changes that contribute to frequency ripples. The traditional control strategy may have sharp frequency changes, while the frequency under the proposed control strategy changes more smoothly. The results show that with a suitable time constant T_J, the frequency fluctuation caused by the load change can be restrained. In addition, the power quality of the microgrid can be improved as well.

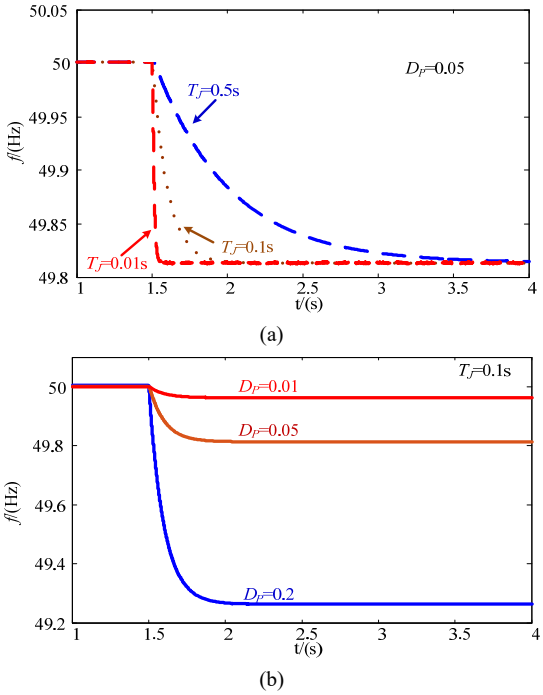

Fig. 7. Frequency reactions of different T_J and D_P.

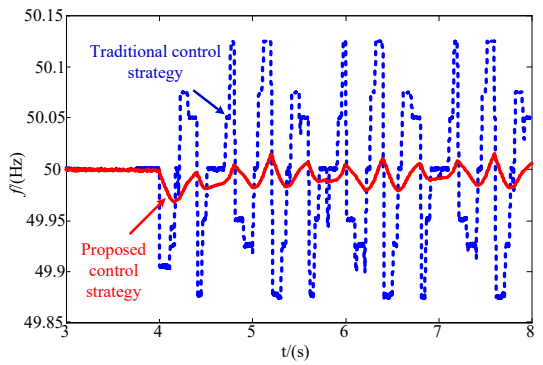

Fig. 8. Frequency response of the traditional and proposed control strategies.

B. In the Grid-Connected Mode

Fig. 9 shows the responses of the inverter system under different grid conditions. The red lines are the equivalent voltages of the inverter as is shown in Fig. 5. The blue lines are the grid voltages. The green lines are the output currents. The equivalent inverter voltage remains unchanged at 200V, 50Hz. The axial voltage regulation part adopts open-loop control. Therefore, it can test the performance of the inverter well. This paper extends the grid transient process to better analyze the inverter actions. Fig. 9(a) shows the system responses when the grid voltage is a normal value (V_{RMS} =200V, f=50Hz). The equivalent voltage v_i is almost the same as v_g, and the output current is nearly zero. There is no power flow when the two voltage sources are almost the same. The ability of transferring desired active and reactive powers under a normal grid voltage has been shown in the Appendix.

When grid fluctuations occur in Fig. 9(b), the voltage falls to 190V, which is 10V lower than standard. The phase of the

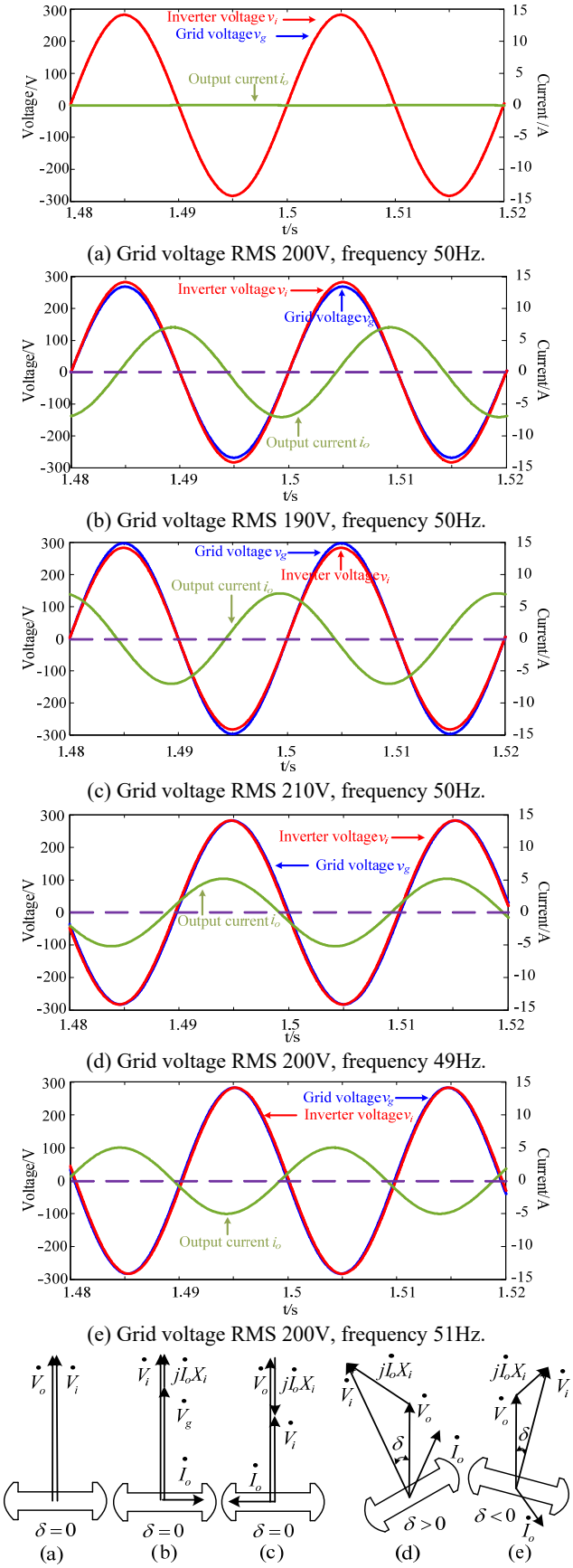

Fig. 9. System response with different grid condition.

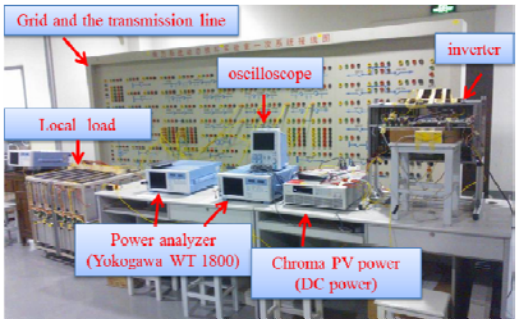

Fig. 10. Layout of the experimental setup.

TABLE II
OUTPUT POWER UNDER DIFFERENT GRID CONDITIONS

Grid Condition	Figure Number	Output P/W	Output Q/Var	PCC Voltage/V
50Hz, 200V	b, e	100.5	-222.8	203.4
49Hz, 200V	a	1002.8	-598.0	204.5
51Hz, 200V	c	-764.0	136.0	201.8
50Hz, 190V	d	235.0	526.9	194.9
50Hz, 210V	f	-42.5	-1039.8	211.9

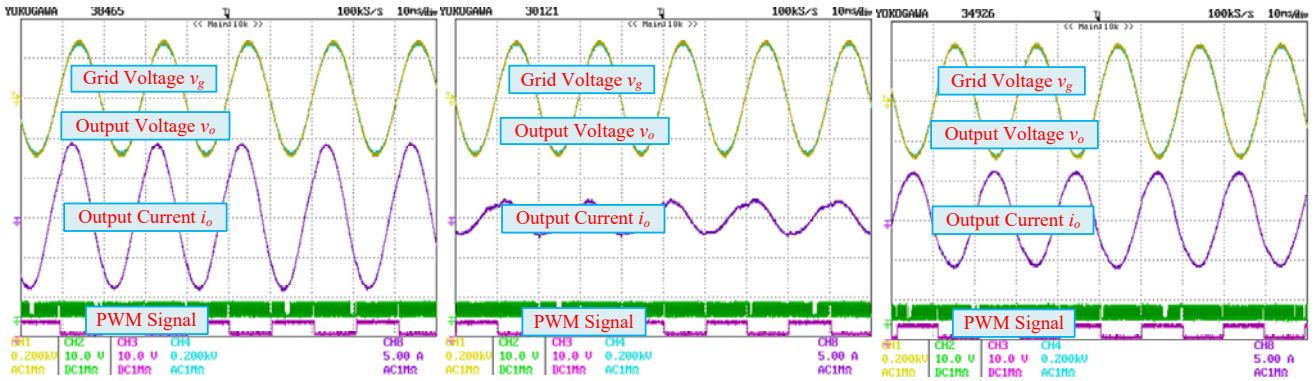

(a) Grid Frequency 49Hz, Grid Voltage 200V. (b) Grid Frequency 50Hz, Grid Voltage 200V. (c) Grid Frequency 51Hz, Grid Voltage 200V.

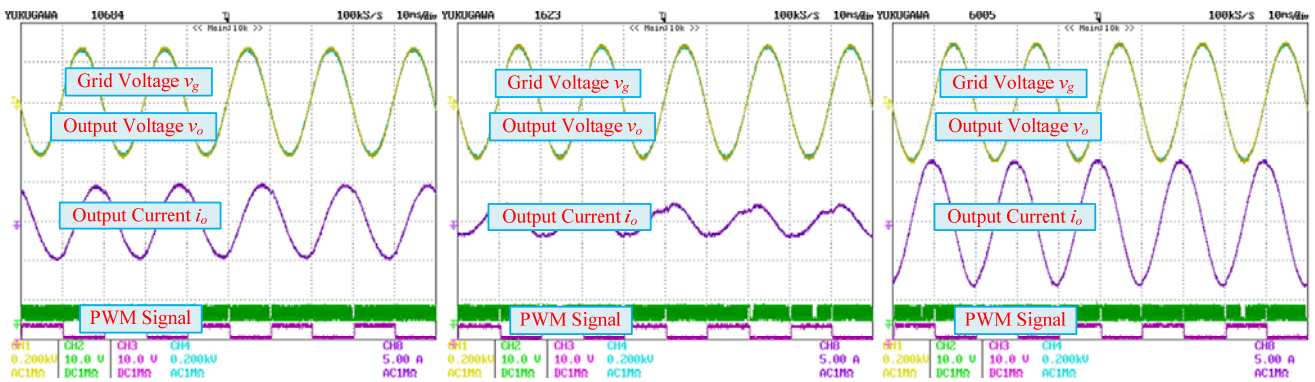

(d) Grid Frequency 50Hz, Grid Voltage 190V. (e) Grid Frequency 50Hz, Grid Voltage 200V. (f) Grid Frequency 50Hz, Grid Voltage 210V.

Fig. 11. Experiment results in different grid conditions.

output current i_o lags and the outputs P and Q are 184W and 930Var, separately. When the grid voltage rises to 210V in Fig. 9(c), the outputs P and Q are -206W and -1024Var, respectively. Therefore, when the grid voltage is lower than normal, the inverter produces reactive power to elevate the grid voltage. Alternatively, when the grid voltage is higher than normal, the inverter absorbs reactive power to reduce the grid voltage. The working statuses are similar to synchronous generators.

When the grid voltage changes to 49Hz, which is 1Hz lower than normal as shown in Fig. 9(d), the outputs P and Q are 711W and -187Var, respectively. When the grid frequency turns to 51Hz, as shown in Fig. 9(e), the outputs P and Q are -691W and 161Var, respectively. The phase of v_i lags and the inverter absorbs active power from the grid when the grid frequency is higher than normal. The phase of v_i leads, and the power flows from the inverter to the grid when the frequency is lower than normal. Simulation results show that the FVCI can work like a synchronous generator that tries to change the grid back to a normal state by adjusting its output active and reactive power. Phasor diagrams in different situations are shown in Fig. 9(f).

Experiments on the proposed control strategy have been carried out as well. The main experimental parameters are the same as those in the simulations. The layout of the experimental setup is shown in Fig. 10. Due to safety considerations, the inverter was connected to the grid with an isolation transformer. Fig. 11 shows the obtained experiment results. Fig. 11 (a), (b), and (c) show the responses of grid frequency variations. Fig. 11 (d), (e), and (f) show the responses of grid voltage amplitude variations. Since the equivalent inverter voltage cannot be measured directly, the

output voltage v_o has been presented in yellow in the results. The output active and reactive powers under different grid conditions are shown in table II. Whenever the grid state is abnormal, the inverter tries to change the voltage back to a normal value. Specifically, when the grid voltage amplitude is abnormal, the inverter produces or absorbs reactive power. When the grid frequency fluctuates, the inverter changes its active power production trying to bring it back to normal. These experimental results show good agreement with the simulation results. The output offsets from the simulation results happen because of the PCC voltage shift.

V. CONCLUSIONS

This paper proposes a flexible control method for a single phase voltage-controlled inverter for microgrids. The proposed strategy makes the inverter equal to a voltage source with a governor-free inner output impedance for power transmission, and own virtual inertia for frequency stability. It can automatically transmit active and reactive power in reaction to different grid conditions. With the designed virtual inertia element, the inverter output voltage frequency fluctuation has been effectively restrained. The realization process was mathematically analyzed and the principal equations to design the inverter were given. With these grid-friendly characteristics, the inverter can be widely used in future power grids. Simulation and experimental results under different situations have been presented to verify the idea.

APPENDIX

Eqn. 12 shows the expressions of the inverter output power when connecting with a grid. Thus, E_i and δ are the main control parameters that determine the output power. The inverter output frequency ω_i is finally the same as the grid frequency ω_g. The steady states of the E_i and δ expressions can be written as follows according to Eqn.8 and 21.

$$E_i = \frac{E + K_{m1}V_1^*}{1+K_{m1}} \tag{27}$$

$$\delta = \frac{K_{m2}}{(1-K_{m2})V_o}V_2^* \tag{28}$$

E_i and δ are controlled separately by different axial voltage regulators V_1^* and V_2^*. The partial derivatives of the output P are Q are obtained from equations 27 and 28 to evaluate the control impact of the regulators.

$$\begin{aligned}\partial P &= \frac{E_i V_o \cos\delta}{X}\partial\delta + \frac{V_o \sin\delta}{X}\partial E_i \\ &= \frac{V_o \sin\delta}{X} * \frac{K_{m1}}{1+K_{m1}}\partial V_1^* + \frac{E_i \cos\delta}{X} * \frac{K_{m2}}{1-K_{m2}}\partial V_2^* \\ \partial Q &= \frac{V_o \cos\delta}{X}\partial E_i - \frac{E_i V_o \sin\delta}{X}\partial\delta\end{aligned} \tag{29}$$

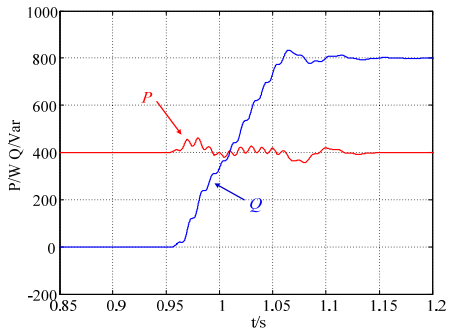

(a)

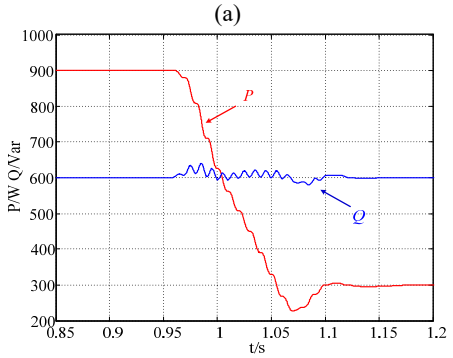

(b)

Fig. 12. Decoupling effect of the output the PQ.

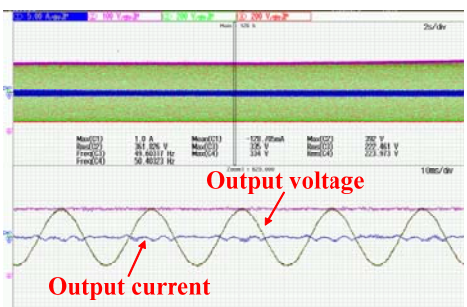

(a) P_{ref} = 0, Q_{ref} = 0.

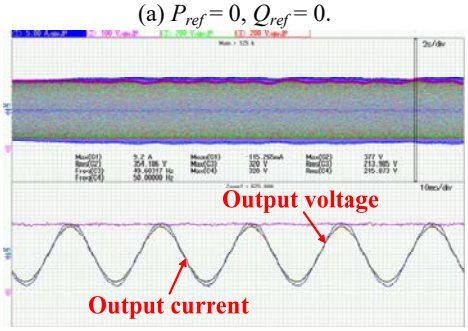

(b) P_{ref} =900W, Q_{ref} = 0.

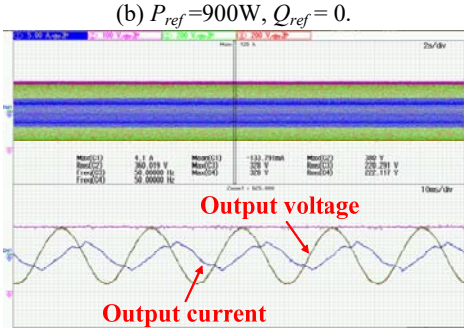

(c) P_{ref}=0, Q_{ref} =600Var.

Fig. 13. Experimental results.

$$= \frac{V_o \cos\delta}{X} * \frac{K_{m1}}{1+K_{m1}} \partial V_1^* - \frac{E_i \sin\delta}{X} * \frac{K_{m2}}{1-K_{m2}} \partial V_2^* \quad (30)$$

Since δ is very small, the above equations show that V_1^* can control the output reactive power, while V_2^* controls output active power [20]. Fig. 12 shows the decouple control of the PQ output.

The change of output P (Q) has little influence on output Q (P). The output voltage and current both transit very smoothly when the PQ references change. The output power decouples well. Fig. 13 shows experimental results of the inverter output voltage and current when transferring desired power to the grid.

ACKNOWLEDGMENT

The authors would like to thank for the financial support of Natural Science Foundation of Shanghai (*Grant No. 16ZR1413000*), Shanghai Engineering Research Center of Green Energy Grid-Connected Technology (*Grant No.13DZ2251900*)

REFERENCES

[1] D. E. Olivares, A. Mehrizi-Sani, A. H. Etemadi, C. A. Canizares, R. Iravani, M. Kazerani, A. H. Hajimiragha, O. Gomis-Bellmunt, M. Saeedifard, R. Palma-Behnke, G. A. Jimenez-Estevez, and N. D. Hatziargyriou, "Trends in microgrid control," *IEEE Trans. Smart Grid*, Vol. 5, No. 4, pp. 1905-1919, Apr. 2014.

[2] J. M. Guerrero, F. Blaabjerg, T. Zhelev, K. Hemmes, E. Monmasson,S. Jemei, M. P. Comech, R. Granadino, and J. I. Frau, "Distributed generation: Toward a new energy paradigm," *IEEE Mag. Ind. Electron.*, Vol. 4, No. 1, pp. 52-64, Mar. 2010.

[3] X. Q. Li, X. J. Wu, Y. W. Geng, and Q. Zhang, "Stability analysis of grid-connected inverters with an LCL filter considering grid impedance," *Journal of Power Electronics*, Vol. 13, No. 5, pp. 896-908 , Sep. 2013.

[4] S. Rakibuzzaman, M. Nadarajah, S. Arthit, and K. Y. Lee. "Impact of large-scale PV penetration on power system oscillatory stability." in *Proc. PESG*, pp. 1-7, 2010.

[5] J. Rocabert, A. Luna, F. Blaabjerg, and P. Rodríguez, "Control of power converters in AC microgrids." *IEEE Trans. Power Electronics*, Vol. 27, No. 11 pp. 4734-4749, Nov. 2012.

[6] S. Riverso, F. Sarzo and G. Ferrari-Trecate, "Plug-and-play voltage and frequency control of islanded microgrids with meshed topology." *IEEE Trans. Smart Grid*, Vol. 6, No. 3, pp. 1176-1184, May 2015.

[7] S. Adhikari and F. Li, "Coordinated Vf and PQ control of solar photovoltaic generators with MPPT and battery storage in microgrids." *IEEE Trans. Smart Grid*, Vol. 5, No. 3, pp 1270-1281, Mar. 2014.

[8] G. Buticchi, M. Liserre, D. Barater, C. Concari, A. Soldati, and G. Franceschini, "Frequency-based control of a micro-grid with multiple renewable energy sources." in *Proc. ECCE*, pp. 5273-5280, 2014.

[9] T. B. Lazzarin, G. A. T. Bauer, and I. Barbi, "A control strategy for parallel operation of single-phase voltage source inverters: analysis, design and experimental results," *IEEE Trans. Ind. Electron.*, Vol. 60, No. 6, pp. 2194-2204, Jul. 2013.

[10] J. C. Vasquez, J. M. Guerrero, M. Savaghebi, J. Eloy-Garcia, and R. Teodorescu, "Modeling, analysis, and design of stationary-reference-frame droop-controlled parallel three-phase voltage source inverters," *IEEE Trans. Ind. Electron.*, Vol. 60, No. 4, pp. 1271-1280, Apr. 2013

[11] J. H. Im, S. H. Song, and S. Kang. "Analysis and compensation of PCC voltage variations caused by wind turbine power fluctuations," *Journal of Power Electronics*, Vol. 13, No. 5, pp. 854-860,Oct. 2013.

[12] J. M. Guerrero, J. Matas, L. Garcia de Vicuna, M. Castilla, and J. Miret, "Decentralized control for parallel operation of distributed generation inverters using resistive output impedance," *IEEE Trans. Ind. Electron.*, Vol. 54, No. 2, pp. 994-1004, Feb. 2007.

[13] G. Fang and M. R. Iravani. "A control strategy for a distributed generation unit in grid-connected and autonomous modes of operation." *IEEE Trans. Power Del.,* Vol. 23, No. 2, pp. 850-859, Feb. 2008.

[14] Q. C. Zhong and G. Weiss, "Synchronverters: Inverters that mimic synchronous generators." *IEEE Trans. Ind. Electron.*, Vol. 58, No. 4, pp. 1259-1267, Apr. 2011.

[15] J. F. Hu, J. G. Zhu, D. G. Dorrell, and J. M. Guerrero. "Virtual flux droop method – A new control strategy of inverters in microgrids." *IEEE Trans. Power Electron.*, Vol. 29, No. 9, pp. 4704-4711, Sep. 2014.

[16] J. W. He and Y. W. Li, "Analysis, design, and implementation of virtual impedance for power electronics interfaced distributed generation," *IEEE Trans. Ind. Appl.*, Vol. 47, No. 6, pp. 2525-2538, Nov. 2011.

[17] J. W. He and Y. W. Li. "Generalized closed-loop control schemes with embedded virtual impedances for voltage source converters with LC or LCL filters." *IEEE Trans. Power Electronics*, Vol. 27, No. 4, pp. 1850-1861, Apr. 2012.

[18] Y. W. Li and C. N. Kao. "An accurate power control strategy for power-electronics-interfaced distributed generation units operating in a low-voltage multibus microgrid," *IEEE Trans. Power Electron.*, Vol. 24, No. 12, pp. 2977-2988, Dec. 2009.

[19] J. B. Zhao, U. Shuuichi, and O. Masaaki, "Grid-connected inverter with inner output impedance and governor-free characteristics." in *Proc. ECCE*, 2010, pp. 586-593.

[20] Y. Chen, J. B. Zhao, K. Q. Qu, and F. Li, "PQ control of micro grid inverter with axial voltage regulators," *Journal of Power Electronics*, Vol. 15, No. 6, pp.1601-1608, Nov. 2015.

Shuaitao Zhang was born in Henan, China, in 1990. He received his B.S. degree in Electrical Engineering from the North China University of Water Resources and Electric Power, Henan, China, in 2013. He is presently working towards his M.S. degree at the Shanghai University of Electric Power, Shanghai, China. His current research interests include the modeling and analysis of inverters and the grid-connected control of renewable energy power generation.

Jinbin Zhao (M'06) was born in Hubei, China, in 1972. He received his M.S. and Ph.D. degrees in Electrical Engineering from Oita University, Oita, Japan, in 2002 and 2005, respectively. He worked as a Researcher in the R&D Headquarters of the Origin Electric Co., Ltd., Tokyo, Japan, from 2005 to 2011. He is presently working as a Professor at the Shanghai University of Electric Power, Shanghai, China. His current research interests include the control of power converters, soft-switching power converters, inverters, distributed power systems, power-factor correction, and electric drive systems. Dr. Zhao is a member of the IEEJ and IEICE of Japan as well as a senior member of the CPSS.

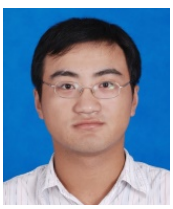

Yang Chen was born in Jiangsu, China, in 1990. He received his B.S. degree in Electrical Engineering from Zhejiang University, Zhejiang, China, in 2012. He worked as an Engineer at Nari-Relays Corporation, Nanjing, China, from 2012 to 2013. He is presently working towards his M.S. degree at the Shanghai University of Electric Power, Shanghai, China. His current research interests include the modeling and control of inverters and distributed power generation in microgrids.

Chaojie He was born in Zhejiang, China, in 1990. He received his B.S. degree in Electrical Engineering and Automation from Hangzhou Dianzi University, Zhejiang, China, in 2013. He is presently working towards his M.S. degree in Electrical Engineering at the Shanghai University of Electric Power, Shanghai, China. His current research interests include grid-connected inverter control and renewable energy generation systems.